Atmospheric
Measurement
Techniques
Discussions

1   CFC-11, CFC-12 and HCFC-22 ground-based remote sensing FTIR measurements at Reunion
2   Island and comparisons with MIPAS/ENVISAT data
3

4   Minqiang Zhou[1,2,3], Corinne Vigouroux[2], Bavo Langerock[2], Pucai Wang[1], Geoff Dutton[4], Christian
5   Hermans[2], Nicolas Kumps[2], Jean-Marc Metzger[5], Geoff Toon[6] , Martine De Mazière[2]
6

7   1. Key Laboratory of Middle Atmosphere and Global Environment Observation, Institute of Atmospheric Physics,
8   Chinese Academy of Sciences, Beijing, China
9   2. Royal Belgian Institute for Space Aeronomy, Brussels, Belgium
10   3. University of Chinese Academy of Sciences, Beijing, China
11   4. Earth System Research Laboratory, NOAA, Boulder, Colorado, USA
12   5. UMS 3365 – OSU Réunion, Université de La Réunion, St-Denis de La Réunion, France
13   6. Jet Propulsion Laboratory, California Institute of Technology, Pasadena, CA, 91109, USA

14   **Abstract**

15   Profiles of CFC-11 (CCl_3F), CFC-12 (CCl_2F_2) and HCFC-22 (CHF_2Cl) have been obtained
16   from Fourier transform infrared (FTIR) solar absorption measurements above the Saint-Denis (St
17   Denis) and Maïdo sites at Reunion Island (21°S, 55°E) with low vertical resolution. FTIR profile
18   retrievals are performed by the SFIT4 program and the detail retrieval strategies along with the
19   systematic/random uncertainties of CFC-11, CFC-12, and HCFC-22 are discussed in this study.
20   The FTIR data of all three species are sensitive to the whole troposphere and the lowermost
21   stratosphere, with the peak sensitivity between 5 and 10 km. The trends derived from the
22   combined St Denis and Maïdo FTIR time-series are -0.86±0.12% and 2.75±0.12% for CFC-11 and
23   HCFC-22, respectively, for the period 2004 to 2016 , and -0.76±0.05% for CFC-12 for 2009 to
24   2016. These measurements are consistent with the trends observed by the National Oceanic and
25   Atmospheric Administration (NOAA) Global Monitoring Division's (GMD) Halocarbons & other
26   Atmospheric Trace Species Group (HATS) measurements at Samoa (14.2°S, 170.5°W) for
27   CFC-11 (-0.87±0.04%), but slightly weaker for HCFC-22 (3.46±0.05%) and stronger for CFC-12
28   (-0.60±0.02%).
29   The ground-based FTIR data have also been compared with the collocated Michelson
30   Interferometer for Passive Atmospheric Sounding (MIPAS/ENVISAT) data, and found to be in
31   good agreement: the observed mean relative biases and standard deviations of the differences
32   between the smoothed MIPAS and FTIR partial columns (6-30 km) are (-4.3% and 4.4%), (-2.9%
33   and 4.6%) and (-0.7% and 6.0%) for CFC-11, CFC-12, and HCFC-22, respectively, which are
34   within the combined error budgets from both measurements.

35   **1. Introduction**

36   CFC-11 (CCl_3F), CFC-12 (CCl_2F_2) and HCFC-22 (CHF_2Cl) are the major sources of chlorine
37   in the stratosphere after photolytic decomposition, and therefore play an important role in
38   stratospheric ozone depletion (Molina and Rowland, 1974). In addition, these gases absorb
39   thermal infrared radiation and contribute significantly to the greenhouse effect (Lashof and Ahuja,
40   1990). Due to the long lifetime of these gases (CFC-11 : ~60 years ; CFC-12: ~120 years;

Atmospheric
Measurement
Techniques
Discussions

41 HCFC-22: ~12 years (Ko et al., 2013)), they are good tracers to study transport and mixing
42 processes in the upper troposphere and lower stratosphere region (Hoffmann and Riese, 2004).
43   Because of the vital importance of these gases, the Advanced Global Atmospheric Gases
44 Experiment (AGAGE) in-situ network has been measuring CFC-11 and CFC-12 continuously
45 since 1978 and HCFC-22 since the 1990s (Cunnold et al., 1997; Dunse et al., 2005). NOAA's
46 Halocarbons & other Atmospheric Trace Species Group (HATS) sampling network started
47 monitoring CFCs from flask grab samples in 1977 and via online in-situ techniques starting in
48 1977 (Elkins et al., 1993). HCFC-22 was added to the NOAA/HATS measurements in 1992.
49 Because of the use of chlorofluorocarbon (CFCs) as propellant and refrigerant in the 1980s, the
50 in-situ measurements show the rapid rise of CFC-11 and CFC-12 at that time. To reduce
51 substances that deplete the ozone layer, amongst others CFCs, 27 nations around the world signed
52 a global environmental treaty, the Montreal Protocol, on September, 1987 (Murdoch and Sandler,
53 1997). The hydrochlorofluorocarbons (HCFCs) were applied to replace the CFCs after the
54 Montreal Protocol, since they react with tropospheric hydroxyl (OH), resulting in a shorter
55 lifetime compared with CFCs. As a result, accelerated increases are observed for HCFCs since
56 2004 in the global atmosphere (Montzka et al., 2009). The tropospheric concentrations of CFC-11
57 and CFC-12 reached their maximums in 1992 and 2003 respectively, and a decline has been
58 observed since then (Elkins et al., 1993; Montzka et al., 1996; Walker et al., 2000).
59   Apart from the in-situ measurements, observations of CFCs and HCFCs abundances have
60 also been made using remote sensing infrared spectroscopy techniques. Space-based observations
61 provide the global distributions and trends of CFCs and HCFCs; examples are the measurements
62 of CFC-11 and CFC-12 from ILAS (Improved Limb Atmospheric Spectrometer), of CFC-11,
63 CFC-12, CFC-113, HCFC-22, HCFC-142a and HCFC-142b from ACE-FTS (Atmospheric
64 Chemistry Experiment - Fourier Transform Spectrometer) and of CFC-11, CFC-12 and HCFC-22
65 from MIPAS (Michelson Interferometer for Passive Atmospheric Sounding) (Khosrawi et al.,
66 2004; Hoffmann et al., 2008; Mahieu et al., 2008). Also ground-based FTIR measurements are
67 able to monitor the CFCs and HCFCs (Notholt, 1994), especially at the Swiss Jungfraujoch station
68 (Zander et al., 2005;Mahieu et al., 2010;Mahieu et al., 2013), where comparisons with the
69 ACE-FTS measurements show a good agreement (Mahieu et al., 2015). They can provide long
70 time-series of CFC-11, CFC-12, HCFC-22 total columns and are therefore very good candidates
71 for supporting the evaluation of satellite and model data and for the evaluation of trends: the
72 Jungfraujoch CFC-11, CFC-12, and HCFC-22 time series and trends have been included in the
73 most recent Scientific Assessment of Ozone Depletion (Carpenter et al., 2014).
74   In this study, we provide the first ground-based FTIR time series of CFC-11, CFC-12 and
75 HCFC-22 in the Southern Hemisphere, namely at two stations, both located at Reunion Island
76 (21°S, 55°E): Saint-Denis (St Denis) and Maïdo, and we compare them to MIPAS/ ENVISAT
77 collocated data. Section 2 describes the FTIR experiments at Reunion Island as well as the
78 retrieval strategy for each target CFC along with the uncertainty analysis. In addition, we provide
79 the three species' trends derived from our FTIR time-series and compare them to the trends
80 observed at American Samoa (SMO) from in-situ measurements for CFC-11 and CFC-12 and
81 flask samplings for HCFC-22, which is one of NOAA's baseline observatories (14.2°S, 170.5°W,
82 77m a.s.l.) at a similar latitude as Reunion Island. Vertical profile and partial column comparisons
83 of the FTIR measurements with the MIPAS data are discussed in Sect. 3. Conclusions are drawn
84 in Sect. 4.

Atmospheric
Measurement
Techniques
Discussions

2. Reunion Island FTIR data

2.1 FTIR experiments at Reunion Island

As explained in Baray et al., (2013), the atmospheric observations at Reunion Island are carried out at two sites, namely St Denis (20.90 °S, 55.48 °E, 85 m a.s.l.), close to the coast, and the Maido mountain site (21.07 °S, 55.38 °E, 2155 m a.s.l.). At present, both sites are equipped with a Bruker 125HR FTIR instrument. These FTIR instruments contribute to two important networks: NDACC (Network for the Detection of Atmospheric Composition Change) and TCCON (Total Carbon Column Observing Network) dedicated to greenhouse gas observations. Each network requires a particular spectral coverage (mid-infrared (600-4500 cm^{-1}) in NDACC and near-infrared (4000-8000 cm^{-1}) in TCCON) and therefore a corresponding instrumental configuration (optical filters, beamsplitters and detectors) and operation mode (including spectral resolution). Since March 2013, when the FTIR spectrometer at Maido became operational, the Maido FTIR has been dedicated to NDACC and the St Denis FTIR to TCCON.

2.1.1 La Reunion - St Denis

The Royal Belgian Institute for Space Aeronomy (BIRA-IASB) started the FTIR solar absorption experiments at La Reunion in St Denis in 2002, with a Bruker 120M FTIR spectrometer, first on a campaign basis with campaigns in 2002 (October), 2004 (August to October) and 2007 (May to November), and then in continuous mode since June 2009 (Senten et al., 2008; Vigouroux et al., 2009; Duflot et al., 2010; Vigouroux et al., 2012; Baray et al., 2013). In September 2011, BIRA-IASB started the replacement of the Bruker 120M by a Bruker 125HR: the Bruker 125HR was installed next to the Bruker 120M and both instruments were set up to make collocated measurements until November 2011, when BIRA-IASB disassembled the Bruker 120M. Since then, at St Denis, BIRA-IASB operates only the Bruker 125HR.

Since October 2013 the instrument is primarily dedicated to TCCON measurements and no more NDACC measurements have been made. Because the CFC retrieval windows requires a KBr beamsplitter and a MCT detector (600 to 1400 cm^{-1}), the CFC data presented in this work at Saint-Denis and requiring the NDACC observational configuration cover the August 2004 - November 2011 period.

2.1.2 La Reunion – Maïdo

BIRA-IASB started operating a second Bruker 125HR FTIR spectrometer at the Maïdo observatory in March 2013 and dedicated it primarily to NDACC measurements with MCT and InSb detectors. As such, our CFC time series at Maïdo cover the March 2013 – present time period.

2.2 FTIR retrieval

The NDACC ground-based FTIR experiment observes the absorption of the direct solar radiation with high spectral resolution (0.0035-0.0110 cm^{-1}) and uses the pressure broadening effect of absorption lines to retrieve volume mixing ratio (vmr) profiles of target gases. In this study, the FTIR retrievals are based on an optimal estimation method (Rodgers, 2000), carried out with the SFIT4 algorithm (https://wiki.ucar.edu/display/sfit4), which is an open source code, jointly developed at the NASA Langley Research Center, the National Center for Atmospheric Research (NCAR) and the National Institute of Water and Atmosphere Research (NIWA). The

Atmospheric
Measurement
Techniques

Open Access

Discussions

EGU

126   National Centers for Environmental Prediction (NCEP) provide the 6-hourly pressure and
127   temperature profiles. The difference between NCEP and the balloon sounding measurements
128   above Reunion Island is used to create the systematic and random error covariance matrices of the
129   water vapor and temperature profiles. HBr cell measurements performed on a daily basis to verify
130   the alignment of the instrument and to obtain the instrument line shape (ILS) using the
131   LINEFIT14.5 program (Hase et al., 1999); the ILS is provided as an input parameter in the
132   forward model of SFIT4.

133   **2.2.1   Retrieval strategy**

134   CFC-11, CFC-12 and HCFC-22 have weak absorptions in the infrared spectral range,
135   requiring careful selection of the retrieval spectral windows in order to minimize the interfering
136   absorptions from other species. The microwindows (see Table 1) are the same as in the work of
137   Mahieu et al. (2010), except for CFC-12: the 922.50-923.60 cm^{-1} window is however not
138   appropriate for the humid site of Reunion Island because of the strong water vapor lines present at
139   the edge of the window (922.13 cm^{-1}). To avoid such interferences from water vapor, we prefer to
140   use the 1160.2-1161.4 cm^{-1} for our CFC-12 retrievals at Reunion Island. The left panels in Fig. 1
141   show the typical transmittances along with the absorption lines of the target and interfering species,
142   and the fitting residuals for the CFC-11, CFC-12 and HCFC-22 retrievals at St Denis. The
143   interfering gases are also listed in Table 1: as indicated in the Table, either a full profile retrieval is
144   performed or only a scaling of the a a priori profile (column retrieval).

145   In each microwindow, the background transmittance $\boldsymbol{\beta}$ describes the shape caused by the
146   optics in the instrument (especially the bandpass filter) as a second order polynomial of the
147   wavenumber:

148    $$\boldsymbol{\beta} = \left[1 + a(\mathbf{w} - w_0) + b(\mathbf{w} - w_0)^2\right] / (1 + z_0) \quad (1).$$

149   In Equation (1), a is the slope coefficient, b is the curvature coefficient, w_0 is the first
150   wavenumber in the microwindow (cm^{-1}), $\mathbf{w}$ is the vector of all wavenumber in the microwindow,
151   and z_0 is the zero level offset (zshift). The parameters a, b, and z_0 can be fitted in SFIT4 in
152   addition to the target gases profiles and interfering species profiles or columns. The calculated
153   transmittance $\mathbf{y_c}$ is the result of bringing the background, absorptions and zshift together:

154    $$\mathbf{y_c} = \boldsymbol{\beta} \cdot (\varsigma(\mathbf{t}(\mathbf{w})) + z_0) \quad (2),$$

155   Where $\mathbf{t}(\mathbf{w})$ is the calculated transmittance (after the absorption from each species and solar

156   lines) and $\varsigma(\mathbf{t}(\mathbf{w}))$ is the transmittance after convolution with the ILS. If necessary, a beam

157   correction can also be applied to fitting the baseline of the transmittance in each microwindow. It
158   creates a zshift-like parameter $\mathbf{z_b}$ for the interferogram perturbation (IP) model:

159    $$\mathbf{y_c} = \boldsymbol{\beta}(\varsigma(\mathbf{t}) + z_0 + \mathbf{z_b}) \quad (3),$$

160   SFIT4 uses 4 parameters (A: amplitude; T: period; φ: phase and τ: slope for the amplitude)
161   to retrieve each beam (the maximum number of beams is 20):

162    $$\vartheta = A(1 + \tau(\mathbf{w} - w_0))e^{i(2\pi/T(w-\psi))} \quad (4),$$

163    $$\mathbf{z_b} = \varsigma(\vartheta) \quad (5),$$

Atmospheric
Measurement
Techniques
Discussions

164   Table 1 lists the parameters used for fitting the background in the CFC-11, CFC-12 and
165   HCFC-22 retrievals. Since the retrieval windows of CFC-12 and HCFC-22 are narrow, linear fit is
166   enough to characterize the spectral background (b=0). However, the retrieval window of CFC-11
167   (830-860 cm^{-1}) is very wide and contains several saturated H_2O absorption lines, therefore zshift,
168   slope, and curvature were retrieved together to fit the oscillating shape of the background in the
169   CFC-11 microwindow, and for the CFC-11 retrieval at Maïdo, it turned out necessary to retrieve
170   also one IP-type beam. Together with one IP-type beam, the retrieved CFC-11 total columns at
171   Maïdo show better agreements with MIPAS data and the ground-based HATS SMO in-situ
172   measurements along with a much smaller fitting residual in comparison with without-beam
173   retrievals. Fig. 2 shows the average residual transmittance for the CFC-11 retrievals at Maïdo,
174   with and without fitting a beam parameter. The spikes mainly result from the strong absorption
175   lines of H_2O. The a priori values for the IP beam parameters were obtained by fitting the mean
176   residuals of all without-beam retrievals. It is clear from Fig. 2 that adding one IP-type beam was
177   useful to remove the background oscillation of the residuals at Maïdo. As such oscillation was not
178   found for the St Denis CFC-11 residuals, the beam parameters retrieval was only applied for
179   Maïdo.
180   We use the empirical pseudo-line-lists (PLL) created by G. Toon (details see
181   http://mark4sun.jpl.nasa.gov/pseudo.html) for the CFC-11, CFC-12, HCFC-12 and $COCl_2$
182   spectroscopy, and HITRAN 2012 (Rothman et al., 2013) for the remaining species (see Table 1).
183   The a priori profiles of interfering gases, except H_2O and O_3, are the mean of 1980-2020 monthly
184   data from Whole Atmosphere Community Climate Model (WACCM, version 6,
185   ftp://acd.ucar.edu/user/jamesw/IRWG/2013/WACCM/V6/). In order to reduce the influence of O_3
186   and H_2O uncertainties, preliminarily retrieved profiles of O_3 and H_2O obtained with the settings of
187   Vigouroux et al. (2015) are used, as input for the CFC-11, CFC-12 and HCFC-22 retrievals. The a
188   priori profiles of target species are the mean of 2004-2016 monthly data from WACCM after
189   scaling to the annual mean of ground-based NOAA/HATS SMO flask grab samples and in-situ
190   measurements of 2009 for St Denis and 2014 for Maïdo. As such, the a priori profiles of CFC-11
191   and CFC-12 for St Denis are a little larger than the ones for Maïdo, while the a priori profile of
192   HCFC-22 for St Denis is a little smaller than that for Maïdo (see Fig. 2). However, all the
193   retrievals at St Denis or at Maïdo use the same a priori profiles. The profiles of the three gases
194   decrease rapidly above 20 km and become close to zero vmr values at 30 km for CFC-11, 40 km
195   for CFC-12 and 100 km for HCFC-22.
196   The a priori covariance matrix (regularization matrix) is another important input parameter in
197   the optimal estimation method. Ideally, the diagonal values of covariance matrix represent the
198   natural variability of the gas concentration around the a priori profile. Therefore, in our study,
199   2004-2016 monthly data from WACCM are used to provide the variability for the FTIR retrieval,
200   which agrees with the a priori profile ensemble. The variabilities of CFC-11, CFC-12 and
201   HCFC-22 are then 5%, 2% and 15%, respectively. The gas profile correlation width is set to 4 km
202   from 0 to 100 km in the SFIT4 retrieval, and the retrieved profiles for CFC-11, CFC-12 and
203   HCFC-22 are shown in Fig. 2.
204   Table 1 lists the DOFS of the total columns of CFC-11, CFC-12 and HCFC-22, along with
205   the standard deviation (1σ); they are 1.1 ±0.1, 1.5 ±0.1, 0.9 ±0.1 respectively at St Denis and 1.1 ±0.1,
206   1.6 ±0.1, 1.1 ±0.1 respectively at Maïdo. The right panels of Fig. 1 shows the typical averaging
207   kernels of the CFC-11, CFC-12 and HCFC-22 retrievals at St Denis; they represent the vertical

208 sensitivity of the measurement as a function of altitude. The FTIR retrievals of all three species are
209 sensible to the whole troposphere and the lowermost stratosphere, with the peak sensitivity around
210 5-10 km. We have to keep in mind that the retrieved profiles of CFC-11, CFC-12 and HCFC-22
211 have very poor vertical resolution: the DOFS range from 0.9 to 1.6 and the
212 full widths at half maximum of the averaging kernels are very wide (~8 km).

213 **2.2.2 Error budget**

214 According to the optimal estimation method (Rodgers, 2000), the final state $\hat{x}$ satisfies

215 $\hat{\mathbf{x}} = \mathbf{x}_a + \hat{G}(\mathbf{y} - F(\hat{\mathbf{x}}, \mathbf{b}) + \hat{K}(\hat{\mathbf{x}} - \mathbf{x}_a))$ (6),

216 $\hat{G} = (\mathbf{S}_a^{-1} + \hat{K}^T \mathbf{S}_\varepsilon^{-1} \hat{K})^{-1} \hat{K}^T \mathbf{S}_\varepsilon^{-1}$ (7),

217 where $\mathbf{x}_a$ is the a priori state vector; $\hat{G}$ is the contribution function, indicating the

218 sensitivity of the retrieval to the measurements; $\hat{K}$ is the weighing function, representing the

219 sensitivity of the measurements to the state vector; y is the observed spectrum and $F(\hat{\mathbf{x}}, \mathbf{b})$ is

220 the forward model (with model parameters represented by **b**) evaluated in the final state,; $\mathbf{S}_a$ is

221 the a priori covariance matrix and $\mathbf{S}_\varepsilon$ is the measurement error covariance matrix. If we consider

222 the different uncertainty components , formula (6) can be approximated as,

223
$$\hat{\mathbf{x}} = \mathbf{x}_a + \hat{G}(F(\mathbf{x}_t, \mathbf{b}) + \boldsymbol{\varepsilon}_F + \boldsymbol{\varepsilon}_y + K_b \boldsymbol{\varepsilon}_b - F(\hat{\mathbf{x}}, \mathbf{b}) + \hat{K}(\hat{\mathbf{x}} - \mathbf{x}_a))$$
$$= \mathbf{x}_a + \hat{G}(\hat{K}(\mathbf{x}_t - \hat{\mathbf{x}}) + \hat{K}(\hat{\mathbf{x}} - \mathbf{x}_a)) + \hat{G}(\boldsymbol{\varepsilon}_F + \boldsymbol{\varepsilon}_y + K_b \boldsymbol{\varepsilon}_b)$$
(8),

224 in which, $\mathbf{x}_t$ is the true state of the atmosphere; $\boldsymbol{\varepsilon}_F$ is the forward model error, $\boldsymbol{\varepsilon}_y$ is the

225 measurement noise; $\mathbf{K}_b$ is the sensitivity of the measurements to the forward model parameters

226 $\mathbf{K}_b = \partial \mathbf{F}(\mathbf{x}_t, \mathbf{b}) / \partial \mathbf{b}$. It is worth noting that this equation is approximated using a Newton

227 iterative algorithm, which is also subject to an error, but the convergence criterion guarantees that

228 the iteration error gets smaller than the noise error on the spectrum. So it is ignored.

229 We can rewrite formula (8) as

230 $\hat{\mathbf{x}} - \mathbf{x}_t = (\hat{A} - I_n)(\mathbf{x}_t - \mathbf{x}_a) + \hat{G}(\boldsymbol{\varepsilon}_F + \boldsymbol{\varepsilon}_y + K_b \boldsymbol{\varepsilon}_b)$ (9),

231 where $\hat{A} = \hat{G}\hat{K}$ is the averaging kernel.

232 The first term in the right side of the equation (9) is the smoothing error, the second term
233 contains three parts: the forward model error; the measurement error and the forward model
234 parameters error. The forward model parameters error comes from the atmospheric (temperature, a
235 priori profiles, pressure …), spectroscopic, geometrical and instrumental parameters, which are
236 not included in the state vector, but do have an impact on the forward model calculation. Each
237 error contains both a systematic and a random part.

238 Tables 2 and 3 list the different contributions to the total average retrieval uncertainty , at St
239 Denis and Maïdo, resp., including smoothing, measurement noise, retrieval parameters (slope;
240 curvature; wavenumber shift; zero-level offset (zshift); beam parameters; solar line shift; simple
241 phase correction), interfering species, temperature profile, solar zenith angle (SZA), spectroscopic
242 parameters (line intensity, air-broadened half-width, temperature dependence of the air-broadened
243 half-width). We assume that the measurement and retrieval parameters have very small systematic
244 uncertainties (set to zero in our case) and that the spectroscopic parameters have negligible
245 random errors. Because zshift is in the state vector for CFC-11, the zshift uncertainty is included in
246 retrieval parameters uncertainties but in the model parameters uncertainties for CFC-12 and

247   HCFC-22. The total average systematic/random uncertainties associated with the retrieved
248   columns for CFC-11, CFC-12, and HCFC-22 are 7.0%/2.0%, 1.8%/1.1%, 4.4%/4.5%, respectively,
249   at St Denis and 6.7%/1.6%, 1.8%/1.1%, 4.5%/4.1% respectively at Maïdo. The systematic
250   uncertainties originate mainly in the uncertainties on the spectroscopic parameters, as well as in
251   the temperature uncertainty. The random uncertainty is dominated by the smoothing error, the
252   uncertainty on the SZA and the measurement noise; especially for HCFC-22, the measurement
253   noise error is very significant due to the narrow and weak absorption of HCFC-22 (see the left
254   bottom panel in Fig. 1).

255   **2.2.3 Total column time series**

256   Fig. 4 shows the time series of retrieved total columns of CFC-11, CFC-12 and HCFC-22 at
257   St Denis and Maïdo. together with their uncertainties (in unit of molecules/cm^2). Although the
258   retrievals use the same database of spectra, the numbers of successful retrievals for CFC-11,
259   CFC-12 and HCFC-22 are different. Fig. 4 indicates that the time series of CFC-12 has the largest
260   data density, because the 1160.2-1161.4 cm^{-1} microwindow falls in the middle of the spectrum
261   with high signal to noise ratio (SNR), while the microwindows 830.0-860.0 cm^{-1} and 828.75-829.4
262   cm^{-1} lie in the edge of the spectrum, with lower SNR due to the optical filter shape. Fig. 4 also
263   shows that there is an offset between the total columns of all three species at St Denis and Maïdo,
264   since the altitude of St Denis (85 m a.s.l.) is much lower than that of Maïdo (2155 m a.s.l.),

265   **2.2.4 Trend analysis and seasonal cycle**

266   Because of the different altitudes of St Denis and Maïdo, it is difficult to compare the total
267   columns of St Denis and Maïdo directly. Therefore, for the trend analysis we extract from the
268   profiles at St Denis the partial columns (2.155-100 km) of CFC-11, CFC-12 and HCFC-22. We
269   plot in Fig.5 these partial columns at St Denis (light coral) together with the total columns at
270   Maïdo, and we can see that they are in good agreement. Also shown for comparison in Fig.5, are
271   the in-situ and flask daily mean measurements at SMO. We use the Chromatograph for
272   Atmospheric Trace Species (CATS) in-situ daily mean data for CFC-11 and CFC-12
273   (http://www.esrl.noaa.gov/gmd/hats/insitu/cats/) and the flask data for HCFC-22 (Montzka et al.,
274   1993). The precision of the in-situ and flask measurements is about a few of tenths of a ppt for
275   CFC-11, CFC-12 and HCFC-22. Our FTIR measurements could capture the main trends of these
276   species very well, but the scatters of the FTIR retrievals are much larger than the in-situ
277   measurements mainly due to the larger retrieval uncertainties of the FTIR measurements, and the
278   FTIR columns is also associated with the scatter on the air column (e.g., due to tropopause shifts
279   and P-variations).

280   To derive the secular trends from the FTIR and in-situ measurements daily means Y(t), with t
281   the time in fractional year, we use a regression model that includes a Fourier series (3rd order) to
282   describe the seasonal cycle:

283   $$Y(t) = A_0 + A_1 \cdot t + \sum_{k=1}^{3} A_{2k} \cos(2k\pi t) + A_{2k+1} \sin(2k\pi t) + \varepsilon(t) \quad (10),$$

284   where A_0 is the intercept at t=0, A_1 is the secular (annual) trend, A_2 to A_7 are the seasonal cycle
285   parameters, and $\varepsilon(t)$ are the residuals between the observations and the model. The
286   auto-correlation in the residuals must be taken into account to avoid the underestimation of trend
287   uncertainties. We follow the approach of (Santer et al., 2000), which by combining their Eqs. 3 to
288   6, leads us to the following corrected uncertainty σ_c on the regression parameters:

Atmospheric
Measurement
Techniques
Discussions

289 $\qquad \sigma_c = \sigma_d * \frac{(n-2)}{(n_e-2)}$ (11),

290 with σ_d the uncertainty directly provided by the regression model, n the number of daily means in

291 the Y(t) time-series, and n_e the effective sampling size:

292 $\qquad n_e = n * \frac{1-r}{1+r}$ (12),

293 with r the auto-correlation, with a time-lag of 1,in the residuals.

294 Table 4 gives the annual percent changes and their uncertainties of CFC-11, CFC-12 and

295 HCF-22 (%) from both FTIR at Reunion Island and from the in-situ and flask measurements at

296 SMO. The trends from MIPAS, ACE, and Jungfraujoch FTIR measurements in Carpenter et al.

297 (2014) are also listed in Table 4 for comparison. The ACE-FTS (2004-2010) trends were

298 determined by averaging the mixing ratios in molecule-dependent altitude ranges within tropical

299 occultation (30 °N-30 °S), the MIPAS (2004-2010) trends were calculated by 10-15 km partial

300 column for the 20 °N-20 °S, and Junfraujoch is the total columns of FTIR measurements. The

301 annual percent change, in this study, is defined as the ratio of the annual change to the mean of all

302 the measurements that are used to do the trend analysis. Since the time range of Maïdo

303 measurements only covers about 3 years, we do not perform trend analysis on Maïdo data only.

304 For CFC-11, the total column annual change at St Denis (2004-2011) is -0.69±0.15%, which is

305 slightly weaker than the one derived from SMO measurements (-0.89±0.01%). It is also weaker

306 than the trends reported by MIPAS, ACE, and Jungfraujoch FTIR measurements. However, the

307 annual change of the combined FTIR partial columns at St Denis and total columns at Maïdo

308 (2004-2016) is very close to the SMO measurements (-0.86±0.12% vs. -0.87±0.04%). For CFC-12,

309 the total column annual change at St Denis (2004-2011) is -0.26±0.10%, which is also slightly

310 weaker than the one derived from SMO measurements (-0.37±0.08%), but in agreement within the

311 estimated uncertainties. It is also in agreement with the ACE-FTS and Jungfraujoch reported

312 trends. Fig. 4 shows that the concentration of CFC-12 has a significant trend change around 2004

313 (increasing before 2004 and decreasing after), therefore, it is better to select the data after 2009 to

314 do the trend analysis. The annual change of the combined partial columns at St Denis and total

315 columns at Maïdo (2009-2016) is stronger than that derived from the SMO measurements

316 (-0.76±0.05% vs. -0.60±0.02%). For HCFC-22, the annual change of St Denis partial columns

317 (3.14±0.43%) is close to that reported from ACF-FTS data and Jungfraujoch measurements for

318 approximately the same period, but slightly smaller than that derived from the SMO

319 measurements (4.04±0.06%). The trend of the combined partial columns at St Denis and total

320 columns at Maïdo (2004-2016) is also smaller than that of the SMO measurements (2.75±0.12%

321 vs. 3.46±0.05%).

322 Fig. 6 shows the seasonal cycles of CFC-11, CFC-12 and HCFC-22. The red lines represent

323 the modeled seasonal cycle obtained by Eq. 10 for the 2004-2016 St Denis -Maïdo time-series,

324 and blue lines represent the mean of FTIR measurements for each month during the 2004-2016

325 period, after subtraction of the trend (removing the systematic retrieval error), together with the

326 standard deviation σ on the mean (thin error bars). The standard deviation σ represents the random

327 error of the FTIR retrievals, and the 2 σ error on the mean ($2\sigma \ / \ \sqrt{n}$; n being the number of

328 measurements for each month) is also shown with thick blue lines. For CFC-11 and HCFC-22,

329 there is no obvious seasonal variation, since the uncertainty is very large. However, there is a

330 significant seasonal variation for CFC-12, for which the concentration is highest in March-May

Atmospheric
Measurement
Techniques
Discussions

331   and lowest in September-November.

3.   Comparison with ENVISAT/MIPAS data

3.1 MIPAS introduction

334   ENVISAT was successfully launched into space on March 1, 2002 carrying several sensors,
335   including MIPAS, a cryogenic limb emission Fourier transform spectrometer (FTS) which
336   observes many trace gases from a wide spectrum covering 865-2410 cm^{-1} (Fischer and Oelhaf,
337   1996). The mission ended on 08 April 2012. From July 2002 to March 2004, MIPAS was operated
338   in full spectral resolution (FR) mode (spectral resolution: 0.05 cm^{-1}), covering the altitude range
339   from 6 km to 68 km. Due to the failure of one of the interferometer slides, MIPAS was operated
340   with a reduced spectral resolution (0.121 cm^{-1}), the so-called RR mode, starting January 2005. The
341   RR mode covers the altitude range from 6 km to 70 km (Fischer et al., 2008). In this paper, we use
342   the Institute of Meteorology and Climate Research (IMK) generated MIPAS/ENVISAT products,
343   taken from https://www.imk-asf.kit.edu/english/308.php. The retrieval windows of MIPAS are
344   831.0-853.0 cm^{-1} for CFC-11; 915.0-925.0 cm^{-1} for CFC-12; 803.50-804.75 cm^{-1}, 808.25-809.75
345   cm^{-1}, 820.50-821.12 cm^{-1} and 828.75-829.50 cm^{-1} for HCFC-22. A dedicated spectroscopic
346   database was applied for MIPAS retrieval (Flaud and Teffo, 2003). The detailed MIPAS CFCs
347   retrieval strategies can be found in previous publications (Hoffmann et al., 2005; Kellmann et al.,
348   2012; Chirkov et al., 2016); all the products have been validated to some degree by comparison
349   with other space experiments, air-borne in-situ instruments, ground-based measurements, or
350   independent ENVISAT MIPAS analyses (Hoffmann et al., 2008).

3.2   Vertical profile comparison

352   There is no temporal overlap between MIPAS data and Maïdo measurements, so the MIPAS
353   footprints within ±2°latitude ±5°longitude around St Denis are selected to compare with the St
354   Denis FTIR measurements. The overpass times of MIPAS above Reunion Island are around 6:30
355   and 18:30 UTC, due to the sun-synchronous orbit of ENVISAT. As the FTIR measurements are
356   recorded only during daytime, the MIPAS data around 6:30 UTC are chosen in the following
357   analysis.

358   Fig. 7 shows the comparison of averaged profiles between FTIR measurements and MIPAS
359   data. The individual FTIR-MIPAS data pair was selected when the FTIR measurement and the
360   MIPAS observation were collocated within ±3 hours around 6:30 UTC on the same day. If more
361   than one MIPAS datapoint was found on a given day, the closest (in geodetic distance) MIPAS
362   data point was taken. If more than one FTIR measurement exists on a given day, each FTIR
363   measurement together with the closest MIPAS datapoint will be taken as one individual data pair.
364   In total, there are 60, 86 and 42 FTIR-MIPAS data pairs for CFC-11, CFC-12 and HCFC-22,
365   respectively. It is worth noting that, to account for the sensitivity of the retrieval to the true
366   profiles and to take into account the low vertical resolution of the FTIR retrieved profiles, the
367   MIPAS profile $\hat{x}_{MIPAS}$ is smoothed by the FTIR averaging kernel (AK) A_{FTIR} (Rodgers and
368   Connor, 2003):

369     $$\hat{x}'_{MIPAS} = x_{FTIR}^{apriori} + A_{FTIR}(\hat{x}_{MIPAS} - x_{FTIR}^{apriori}) \quad (13),$$

370   Where $x_{FTIR}^{apriori}$ is the FTIR a priori profile and $\hat{x}'_{MIPAS}$ is the MIPAS profile after

Atmospheric
Measurement
Techniques
Discussions

371   smoothing correction is applied. The MIPAS profile was interpolated onto the FTIR retrieval grids

372   (keeping the total column unchanged). Fig. 7 mainly focuses on the vertical range from 6 to 30 km,

373   because there aren't any MIPAS measurements below 6 km (Fischer et al., 2008) and the FTIR

374   sensitivity is very weak above 30 km (see Fig. 1). In addition, the low FTIR sensitivity above 30

375   km leads to a very small relative difference (less than 1%) between the smoothed MIPAS and

376   FTIR ((MIPAS-FTIR)/FTIR $\times$ 100%) above 30 km for all three species (see right panels in Fig. 7).

377   Since the FTIR retrievals have very poor vertical resolution, the "oscillation" of the profiles of the

378   relative difference between FTIR and MIPAS could be caused by the FTIR retrievals. Anyhow, for

379   CFC-11, the FTIR concentration is larger than the smoothed MIPAS concentration value between

380   6 km and 30 km: the largest difference is of order -7% around 15 km. For CFC-12, the FTIR

381   retrieval is larger below 14 km and smaller above 14 km than the smoothed MIPAS data. The

382   peaks are around 6 km (-8%) and 18 km (2%). For HCFC-22, the FTIR retrieval is very close to

383   the smoothed MIPAS data: the relative difference is within ±5% between 6 and 30 km.

384   **3.3 Partial column comparison**

385   In this section, we compare the MIPAS and St Denis FTIR partial columns (PC) from 6 to 30

386   km, for the same collocated pairs as in Sect. 3.2. The DoFS of the partial columns of CFC-11,

387   CFC-12, HCFC-22 are 0.6±0.1, 0.9±0.1, 0.6±0.1. Table 5 exhibits the statistical values of the

388   comparison: relative bias and standard deviation of the difference between the MIPAS (raw and

389   smoothed) and FTIR, together with the partial column uncertainties from both data sets. The

390   largest mean relative bias is found for CFC-11 (-4.3%), showing that the FTIR partial columns are

391   larger than the MIPAS ones, which is probably caused by the large systematic error of FTIR

392   CFC-11 retrievals (10.5%). For CFC-12, the bias is -2.7% which is also within the uncertainty

393   budget of combined data sets. The lowest relative bias is found for HCFC-22 (-0.7%) but the

394   standard deviation is large (6.0%) because of the large FTIR retrieval errors (7.8%/7.1%) and

395   MIPAS retrieval error (5.0%). Overall, the biases and standard deviations between the two data

396   sets lie within the uncertainty budgets for the three species.

397   Fig. 8 shows the time series of the monthly means of partial columns of CFC-11, CFC-12 and

398   HCFC-22 FTIR measurements at St Denis (grey) along with the raw MIPAS data (red). The

399   smoothed MIPAS data are not shown here, because more than half of MIPAS data do not

400   correspond with an individual FTIR measurement within one day or even one week, and the

401   differences between partial columns of smoothed and unsmoothed data are within 1.0%. Note that

402   the bias between the raw MIPAS and FTIR data also contains the smoothing error, but the bias

403   already lies within the uncertainty budget even without smoothing error (see Table 5). Fig. 8

404   shows that the monthly means of MIPAS and FTIR data are in a good agreement.

405   **4.   Summary**

406   CFC-11, CFC-12 and HCFC-22 mixing ratio profiles were retrieved at Reunion Island from

407   St Denis and Maïdo ground-based solar absorption FTIR measurements between 2004 and 2016.

408   The retrieval microwindows are carefully selected to minimize the interfering absorptions from

409   other species. The averaging kernels of CFC-11, CFC-12 and HCFC-22 are very similar, and the

410   retrieved information comes mainly from the troposphere and lower stratosphere with low vertical

411   resolution. As expected as a response to the Montreal Protocol, negative trends of total columns of

412   CFC-11 and CFC-12 and a positive trend of HCFC-22 were observed at St Denis and Maïdo,

Atmospheric
Measurement
Techniques
Discussions

413 which is in good agreement with the in-situ surface data   and other remote sensing results (E.g.,
414 SMO in-situ and flask measurements and Jungfraujoch FTIR data, resp.). The observed FTIR total
415 column trends above St Denis between 2004 and 2011 are $-0.69\pm0.15\%/yr^{-1}$ for CFC-11,
416 $-0.26\pm0.10\%/ yr^{-1}$ for CFC-12 and $3.14\pm0.43\%/ yr^{-1}$ for HCFC-22. The trends of combined FTIR
417 partial columns (2.155-100 km) at St Denis and total columns at Maïdo are $-0.86\pm0.12\%$ for
418 CFC-11 and $2.75\pm0.12\%$ for HCFC-22 between 2004 and 2016, , and $-0.76\pm0.05\%$ for CFC-12
419 between 2009 and 2016. These trends are consistent with the ones observed at SMO for CFC-11
420 $(-0.87\pm0.04\%)$, but slightly smaller for HCFC-22 $(3.46\pm0.05\%)$ and larger for CFC-12
421 $(-0.60\pm0.02\%)$.

422 The FTIR measurements were also compared with collocated MIPAS/ENVISAT data around
423 St Denis. There are 60, 86 and 42 FTIR-MIPAS collocated data pairs for CFC-11, CFC-12 and
424 HCFC-22 within $\pm2°$ latitude, $\pm5°$ longitude and ±3 hours around 6:30 UTC. The differences
425 between FTIR and smoothed MIPAS profiles from 6 to 30 km altitude are within $\pm10\%$ for
426 CFC-11 and CFC-12, and $\pm5\%$ for HCFC-22. The relative biases and standard deviations of the
427 differences between the partial columns (6-30 km) of smoothed MIPAS and FTIR are -4.3%
428 $\pm4.4\%$, -2.9% $\pm4.6\%$ and -0.7% $\pm6.0\%$ for CFC-11, CFC-12, and HCFC-22, respectively, which lie
429 within the error budgets from both data sets. Overall, the time series of MIPAS monthly partial
430 columns show a good agreement with the St Denis FTIR partial column data.

431 **Acknowledgments**

445

446 **References**

447 Baray, J.-L., Courcoux, Y., Keckhut, P., Portafaix, T., Tulet, P., Cammas, J.-P., Hauchecorne, A.,
448 Godin-Beekmann, S., De Mazière, M., and Hermans, C.: Maïdo observatory: a new high-altitude
449 station facility at Reunion Island (21 °S, 55 °E) for long-term atmospheric remote sensing and in situ
450 measurements, Atmos. Meas. Tech., 6, 2865-2877, 10.5194/amt-6-2865-2013, 2013.
451 Brown, A. T., Chipperfield, M. P., Boone, C., Wilson, C., Walker, K. A., and Bernath, P. F.: Trends in
452 atmospheric halogen containing gases since 2004, J. Quant. Spectrosc. Radiat. Transf., 112, 2552-2566,
453 10.1016/j.jqsrt.2011.07.005, 2011.

Atmospheric
Measurement
Techniques
Discussions

454   Carpenter, L. J., Reimann, S., Burkholder, J. B., Clerbaux, C., Hall, B. D., Hossaini, R., Laube, J. C.,
455   and Yvon-Lewis, S. A.: Update on ozone-depleting substances (ODSs) and other gases of interest to the
456   Montreal protocol, Scientific Assessment of Ozone Depletion: 2014, 2014.
457   Chirkov, M., Stiller, G. P., Laeng, A., Kellmann, S., von Clarmann, T., Boone, C. D., Elkins, J. W.,
458   Engel, A., Glatthor, N., Grabowski, U., Harth, C. M., Kiefer, M., Kolonjari, F., Krummel, P. B., Linden,
459   A., Lunder, C. R., Miller, B. R., Montzka, S. A., Mühle, J., O'Doherty, S., Orphal, J., Prinn, R. G., Toon,
460   G., Vollmer, M. K., Walker, K. A., Weiss, R. F., Wiegele, A., and Young, D.: Global HCFC-22
461   measurements with MIPAS: retrieval, validation, global distribution and its evolution over 2005–2012,
462   Atmos. Chem. Phys., 16, 3345-3368, 10.5194/acp-16-3345-2016, 2016.
463   Cunnold, D., Weiss, R., Prinn, R., Hartley, D., Simmonds, P., Fraser, P., Miller, B., Alyea, F., and Porter,
464   L.: GAGE/AGAGE measurements indicating reductions in global emissions of CCl3F and CCl2F2 in
465   1992–1994, J. Geophys. Res. Atmos., 102, 1259-1269, 10.1029/96JD02973, 1997.
466   Duflot, V., Dils, B., Baray, J. L., De Mazière, M., Attié, J. L., Vanhaelewyn, G., Senten, C., Vigouroux,
467   C., Clain, G., and Delmas, R.: Analysis of the origin of the distribution of CO in the subtropical
468   southern Indian Ocean in 2007, J. Geophys. Res., 115, 10.1029/2010jd013994, 2010.
469   Dunse, B., Steele, L., Wilson, S., Fraser, P., and Krummel, P.: Trace gas emissions from Melbourne,
470   Australia, based on AGAGE observations at Cape Grim, Tasmania, 1995–2000, Atmos. Environ., 39,
471   6334-6344, 10.1016/j.atmosenv.2005.07.014, 2005.
472   Elkins, J., Thompson, T., Swanson, T., Butler, J., Hall, B., Cummings, S., Fisher, D., and Raffo, A.:
473   Decrease in the growth rates of atmospheric chlorofluorocarbons 11 and 12, Nature, 364, 780-783,
474   10.1038/364780a0, 1993.
475   Fischer, H., and Oelhaf, H.: Remote sensing of vertical profiles of atmospheric trace constituents with
476   MIPAS limb-emission spectrometers, Appl. Opt., 35, 2787-2796, 10.1364/AO.35.002787, 1996.
477   Fischer, H., Birk, M., Blom, C., Carli, B., Carlotti, M., Clarmann, T. v., Delbouille, L., Dudhia, A.,
478   Ehhalt, D., and Endemann, M.: MIPAS: an instrument for atmospheric and climate research, Atmos.
479   Chem. Phys., 8, 2151-2188, 10.5194/acp-8-2151-2008, 2008.
480   Flaud, J.-M. P. C., and Teffo, B. P. A. C. L.: Molecular line parameters for the MIPAS (Michelson
481   Interferometer for Passive Atmospheric Sounding) experiment, J. Atmos. Sol.-Terr. Phys., 16, 172-181,
482   2003.
483   Hase, F., Blumenstock, T., and Paton-Walsh, C.: Analysis of the instrumental line shape of
484   high-resolution Fourier transform IR spectrometers with gas cell measurements and new retrieval
485   software, Appl. Opt., 38, 3417-3422, 10.1364/AO.38.003417, 1999.
486   Hoffmann, L., and Riese, M.: Quantitative transport studies based on trace gas assimilation, Adv. Space
487   Res., 33, 1068-1072, 10.1016/S0273-1177(03)00592-1, 2004.
488   Hoffmann, L., Spang, R., Kaufmann, M., and Riese, M.: Retrieval of CFC-11 and CFC-12 from
489   Envisat MIPAS observations by means of rapid radiative transfer calculations, Adv. Space Res., 36,
490   915-921, 10.1016/j.asr.2005.03.112, 2005.
491   Hoffmann, L., Kaufmann, M., Spang, R., Müller, R., Remedios, J. J., Moore, D. P., Volk, C., Clarmann,
492   T. v., and Riese, M.: Envisat MIPAS measurements of CFC-11: retrieval, validation, and climatology,
493   Atmos. Chem. Phys., 8, 3671-3688, 10.5194/acp-8-3671-2008, 2008.
494   Kellmann, S., von Clarmann, T., Stiller, G. P., Eckert, E., Glatthor, N., Höpfner, M., Kiefer, M., Orphal,
495   J., Funke, B., Grabowski, U., Linden, A., Dutton, G. S., and Elkins, J. W.: Global CFC-11 (CCl3F) and
496   CFC-12 (CCl2F2) measurements with the Michelson Interferometer for Passive Atmospheric Sounding
497   (MIPAS): retrieval, climatologies and trends, Atmos. Chem. Phys., 12, 11857-11875,

Atmospheric
Measurement
Techniques
Discussions

498   10.5194/acp-12-11857-2012, 2012.

499   Khosrawi, F., Müller, R., Irie, H., Engel, A., Toon, G., Sen, B., Aoki, S., Nakazawa, T., Traub, W., and

500   Jucks, K.: Validation of CFC‐12 measurements from the Improved Limb Atmospheric Spectrometer

501   (ILAS) with the version 6.0 retrieval algorithm, J. Geophys. Res. Atmos., 109, 10.1029/2003JD004325,

502   2004.

503   Ko, M., Newman, P., Reimann, S., Strahan, S., Plumb, R., Stolarski, R., Burkholder, J., Mellouki, W.,

504   Engel, A., and Atlas, E.: Lifetimes of stratospheric ozone-depleting substances, their replacements, and

505   related species, SPARC Report, 2013.

506   Lashof, D. A., and Ahuja, D. R.: Relative contributions of greenhouse gas emissions to global warming,

507   Nature, 529 - 531, doi:10.1038/344529a0, 1990.

508   Mahieu, E., Duchatelet, P., Demoulin, P., Walker, K., Dupuy, E., Froidevaux, L., Randall, C., Catoire,

509   V., Strong, K., and Boone, C. D.: Validation of ACE-FTS v2. 2 measurements of HCl, HF, CCl 3 F and

510   CCl 2 F 2 using space-, balloon-and ground-based instrument observations, Atmos. Chem. Phys., 8,

511   6199-6221, 10.5194/acp-8-6199-2008, 2008.

512   Mahieu, E., Rinsland, C. P., Gardiner, T., Zander, R., Demoulin, P., Chipperfield, M. P., Ruhnke, R.,

513   Chiou, L. S., and De Mazière, M.: Recent trends of inorganic chlorine and halogenated source gases

514   above the Jungfraujoch and Kitt Peak stations derived from high-resolution FTIR solar observations,

515   Geophys. Res. Abstr., 2010.

516   Mahieu, E., O'Doherty, S., Reimann, S., Vollmer, M., Bader, W., Bovy, B., Lejeune, B., Demoulin, P.,

517   Roland, G., and Servais, C.: First retrievals of HCFC-142b from ground-based high resolution FTIR

518   solar observations: application to high altitude Jungfraujoch spectra, Geophys. Res. Abstr., 2013.

519   Mahieu, E., Bader, W., and Franco, B.: Recent results derived from regular ground-based FTIR

520   observations at the Jungfraujoch and other NDACC stations, ACE Science Team Meeting, 2015.

521   Molina, M. J., and Rowland, F. S.: Stratospheric sink for chlorofluoromethanes: chlorine

522   atom-catalysed destruction of ozone, Nature, 249, 810-812, 10.1038/249810a0, 1974.

523   Montzka, S., Myers, R., Butler, J., Elkins, J., and Cummings, S.: Global tropospheric distribution and

524   calibration scale of HCFC‐22, Geophys. Res. Lett., 20, 703-706, 10.1029/93GL00753, 1993.

525   Montzka, S., Hall, B., and Elkins, J.: Accelerated increases observed for hydrochlorofluorocarbons

526   since 2004 in the global atmosphere, Geophys. Res. Lett., 36, 10.1029/2008GL036475, 2009.

527   Montzka, S. A., Butler, J. H., Myers, R. C., Thompson, T. M., Swanson, T. H., Clarke, A. D., Lock, L.

528   T., and Elkins, J. W.: Decline in the tropospheric abundance of halogen from halocarbons: Implications

529   for stratospheric ozone depletion, Science, 272, 1318-1322, 10.1126/science.272.5266.1318, 1996.

530   Murdoch, J. C., and Sandler, T.: The voluntary provision of a pure public good: The case of reduced

531   CFC   emissions   and   the   Montreal   Protocol,   J.   Public.   Econ.,   63,   331-349,

532   10.1016/S0047-2727(96)01598-8, 1997.

533   Notholt, J.: FTIR measurements of HF, N2O and CFCs during the Arctic polar night with the moon as

534   light   source,   subsidence   during   winter   1992/93,   Geophys.   Res.   Lett.,   21,   2385-2388,

535   10.1029/94GL02351, 1994.

536   Rodgers, C. D.: Inverse methods for atmospheric sounding: theory and practice, World scientific

537   Singapore, 2000.

538   Rodgers, C. D., and Connor, B. J.: Intercomparison of remote sounding instruments, J. Geophys. Res.,

539   108, 10.1029/2002jd002299, 2003.

540   Rothman, L. S., Gordon, I. E., Babikov, Y., Barbe, A., Benner, D. C., Bernath, P. F., Birk, M., Bizzocchi,

541   L., Boudon, V., Brown, L. R., Campargue, A., Chance, K., Cohen, E. A., Coudert, L. H., Devi, V. M.,

Atmospheric
Measurement
Techniques

Open Access

EGU

Discussions

542 Drouin, B. J., Fayt, A., Flaud, J.-M., Gamache, R. R., Harrison, J. J., Hartmann, J.-M., Hill, C., Hodges,
543 J. T., Jacquemart, D., Jolly, A., Lamouroux, J., Roy, R. J. L., Li, G., Long, D. A., Lyulin, O. M., Mackie,
544 C. J., Massie, S. T., Mikhailenk, S., Müller, H. S. P., Naumenko, O. V., and Nikitin, A. V.: The
545 HITRAN2012 molecular spectroscopic database, J. Quant. Spectrosc. Radiat. Transf.,
546 10.1016/j.jqsrt.2013.07.002, 2013.
547 Santer, B. D., Wigley, T., Boyle, J., Gaffen, D. J., Hnilo, J., Nychka, D., Parker, D., and Taylor, K.:
548 Statistical significance of trends and trend differences in layer‐average atmospheric temperature time
549 series, J. Geophys. Res. Atmos., 105, 7337-7356, 10.1029/1999JD901105, 2000.
550 Senten, C., Mazière, M. D., Dils, B., Hermans, C., Kruglanski, M., Neefs, E., Scolas, F., Vandaele, A.
551 C., Vanhaelewyn, G., and Vigouroux, C.: Technical Note: New ground-based FTIR measurements at Ile
552 de La Réunion: observations, error analysis, and comparisons with independent data, Atmos. Chem.
553 Phys., 8, 3483-3508, 10.5194/acp-8-3483-2008, 2008.
554 Vigouroux, C., Hendrick, F., Stavrakou, T., Dils, B., Smedt, I. D., Hermans, C., Merlaud, A., Scolas, F.,
555 Senten, C., and Vanhaelewyn, G.: Ground-based FTIR and MAX-DOAS observations of formaldehyde
556 at Réunion Island and comparisons with satellite and model data, Atmos. Chem. Phys., 9, 9523-9544,
557 10.5194/acp-9-9523-2009, 2009.
558 Vigouroux, C., Stavrakou, T., Whaley, C., Dils, B., Duflot, V., Hermans, C., Kumps, N., Metzger, J. M.,
559 Scolas, F., Vanhaelewyn, G., Müller, J. F., Jones, D. B. A., Li, Q., and De Mazière, M.: FTIR
560 time-series of biomass burning products (HCN, C2H6, C2H2, CH3OH, and HCOOH) at Reunion
561 Island (21 ° S, 55 ° E) and comparisons with model data, Atmos. Chem. Phys., 12, 10367-10385,
562 10.5194/acp-12-10367-2012, 2012.
563 Vigouroux, C., Blumenstock, T., Coffey, M., Errera, Q., García, O., Jones, N. B., Hannigan, J. W., Hase,
564 F., Liley, B., Mahieu, E., Mellqvist, J., Notholt, J., Palm, M., Persson, G., Schneider, M., Servais, C.,
565 Smale, D., Thölix, L., and De Mazière, M.: Trends of ozone total columns and vertical distribution
566 from FTIR observations at eight NDACC stations around the globe, Atmos. Chem. Phys., 15,
567 2915-2933, 10.5194/acp-15-2915-2015, 2015.
568 Walker, S., Weiss, R., and Salameh, P.: Reconstructed histories of the annual mean atmospheric mole
569 fractions for the halocarbons CFC-11 CFC-12, CFC-113, and carbon tetrachloride, J. Geophys. Res.
570 Oceans, 105, 14285-14296, 10.1029/1999JC900273, 2000.
571 Zander, R., Mahieu, E., Demoulin, P., Duchatelet, P., Servais, C., Roland, G., Delbouille, L., De
572 Mazière, M., and Rinsland, C. P.: Evolution of a dozen non-CO2 greenhouse gases above Central
573 Europe since the mid-1980s, Environ. Sci., 2, 295-303, 10.1080/15693430500397152, 2005.
574 Zander, R., Mahieu, E., Demoulin, P., Duchatelet, P., Roland, G., Servais, C., De Mazière, M., Reimann,
575 S., and Rinsland, C. P.: Our changing atmosphere: Evidence based on long-term infrared solar
576 observations at the Jungfraujoch since 1950, Sci. Total Environ., 391, 184-195,
577 10.1016/j.scitotenv.2007.10.018, 2008.
578

Atmospheric
Measurement
Techniques
Open Access
Discussions
EGU

579   Table 1. Microwindows, interfering gases, spectroscopic database, a priori profile and background

580   parameters (slope, curvature, zshift and beam as discussed in Section 2.2.1) used for the SFIT4

581   retrievals of CFC-11, CFC-12 and HCFC-22. The degree of freedom (DOF, mean and standard

582   deviation) of retrievals at St Denis and Maïdo.

Target gas	CFC-11 (CCl_3F)	CFC-12 (CCl_2F_2)	HCFC-22 (CHF_2Cl)
Microwindows (cm^{-1})	830.0-860.0	1160.2-1161.4	828.75-829.4
Profile retrieval	CFC-11, H_2O	CFC-12, N_2O	HCFC-22
Column retrieval	HNO_3 O_3 $COCl_2$ CO_2	O_3 CH_4 H_2O	CO_2 H_2O O_3
Spectroscopy	PLL, HITRAN2012	PLL, HITRAN2012	PLL, HITRAN2012
A priori profile	WACCM	WACCM	WACCM
St Denis background	slope, curvature, zshift	slope	slope
Maïdo background	slope, curvature, zshift, beam	slope	slope
DOFS (St Denis)	1.1 ±0.1	1.5 ±0.1	0.9 ±0.1
DOFS (Maïdo)	1.0 ±0.1	1.6 ±0.1	1.1 ±0.1

583

Atmospheric
Measurement
Techniques

Open Access

Discussions

EGU

584   Table 2. Systematic and random uncertainties (in %) for CFC-11, CFC-12, and HCFC-22 at St

585   Denis. Sb represents the relative uncertainties of the non-retrieved parameters. For temperature,

586   the systematic/random Sb matrix was created by the mean/standard deviation of the differences

587   between NCEP and the balloon observations. For the spectroscopic parameters, 0.07, 0.01 and

588   0.05 are the relative uncertainties of CFC-11, CFC-12 and HCFC-22, which are according to the

589   PLL database, respectively. When a relative uncertainty is smaller than 0.01%,   it is considered

590   negligible and represented as "-". For zshift, the same uncertainty is adopted for the systematic

591   and random error; zshiftis included in the retrieval parameters for CFC-11, but not for CFC-12 and

592   HCFC-22.For SZA, the systematic uncertainty is 0.001 and the random uncertainty is 0.002 (in the

593   bracket).

Error	Sb	CFC-11		CFC-12		HCFC-22	
		Systematic	Random	Systematic	Random	Systematic	Random
Smoothing		0.18	1.03	0.18	0.79	0.47	0.51
Measurement		-	0.80	-	0.21	-	4.05
Retrieval parameters		-	-	-	-	-	0.51
Interfering species		0.12	0.84	-	0.10	0.02	0.13
Temperature		1.35	0.30	0.87	0.15	1.00	0.18
SZA	0.001(0.002)	0.21	0.42	0.36	0.72	0.63	1.26
Line intensity	0.07/0.01/0.05	6.59	-	1.00	-	3.96	-
T-dependence of line width	0.07/0.01/0.05	-	-	-	-	0.15	-
Air-broadening of line width	0.07/0.01/0.05	0.45	-	0.07	-	1.53	-
szshift	0.01	-	-	0.12	0.09	0.10	0.12
Total		7.0	2.0	1.8	1.1	4.4	4.5

594

Atmospheric
Measurement
Techniques
Discussions

595   Table 3. Same as Table 2, but for Maïdo.

Error	Sb	CFC-11		CFC-12		HCFC-22	
		Systematic	Random	Systematic	Random	Systematic	Random
Smoothing		0.23	0.90	0.02	0.67	0.40	0.58
Measurement		-	0.70	-	0.20	-	3.36
Retrieval parameters		-	0.26	-	-	-	0.12
Interfering species		0.08	0.20	-	-	0.03	0.03
Temperature		1.82	0.76	1.02	0.19	0.84	0.16
SZA	0.001(0.002)	0.25	0.51	0.22	0.44	0.22	0.44
Line intensity	0.07/0.01/0.05	6.22	-	0.98	-	4.22	-
T-dependence of line width	0.07/0.01/0.05	0.05	-	-	-	0.05	-
Air-broadening of line width	0.07/0.01/0.05	1.54	-	0.05	-	1.48	-
zshift	0.01	-	-	0.12	0.07	0.10	0.05
Total		6.7	1.6	1.8	1.1	4.5	3.6

596

Atmospheric
Measurement
Techniques
Open Access
Discussions
EGU

597   Table 4. The annual percent changes (in %/year, relative to the mean of data used in the trend

598   analysis) and uncertainties of FTIR total columns of CFC-11, CFC-12 and HCF-22 at St Denis

599   (2004-2011) and of the combined partial columns (2.155-100 km) at St Denis along with the total

600   columns at Maïdo (2004-2016 for CFC-11 and HCFC-12, and 2009-2016 for CFC-12). The trends

601   from in-situ and flask measurements at SMO are also given for the same time periods. The trends

602   observed by MIPAS (2004-2010), ACE-FTS (2004-2010) and by the ground-based FTIR at

603   Jungfraujoch (2004-2010) % in %/yr relative to the 2007 annual mean are taken from Carpenter et

604   al. (2014) as described in the text.

Dataset	Time range	CFC-11	CFC-12	HCFC-22	Reference
St Denis (TC)	2004-2011	-0.69 ±0.15	-0.26 ±0.10	3.14 ±0.43	
SMO	2004-2011	-0.89 ±0.01	-0.37 ±0.08	4.04 ±0.06	
MIPAS	2004-2010	-1.03 ±0.09	-0.51 ±0.09	-	Kellmann et al., 2012
ACE-FTS	2004-2010	-0.9 ±0.1	-0.4 ±0.1	3.7 ±0.1	Brown et al., 2011
Jungfraujoch	2004-2010	-0.99 ±0.10	-0.38 ±0.07	3.52 ±0.08	Zander et al., 2008
St Denis(PC) + Maïdo(TC)	2004-2016	-0.86 ±0.12	-	2.75 ±0.12	
	2009-2016	-	-0.76 ±0.05	-	
SMO	2004-2016	-0.87 ±0.04	-	3.46 ±0.05	
	2009-2016	-	-0.60 ±0.02	-	

605

Atmospheric
Measurement
Techniques

Open Access

Discussions

EGU

606 Table 5. The number of collocated MIPAS-FTIR pairs, bias and standard deviation (std) of the
607 relative differences ((MIPAS-FTIR)/FTIR×100%) between the partial columns (6-30 km) of
608 MIPAS (both the raw and smoothed data) and FTIR, together with the mean random and
609 systematic uncertainties of the FTIR partial columns and the retrieval error of the MIPAS data
610 (in %).

	CFC-11	CFC-12	HCFC-22
Number of data pairs	60	86	42
Bias_raw	-4.4	-3.3	0.2
Std_raw	4.7	4.5	6.3
Bias_smoothed	-4.3	-2.9	-0.7
Std_smoothed	4.4	4.6	6.0
FTIR PC random error	4.2	3.5	7.8
FTIR PC systematic error	10.5	2.6	7.1
MIPAS PC retrieval error	4.1	4.3	5.0

611

Atmospheric
Measurement
Techniques
Discussions

Open Access

EGU

612
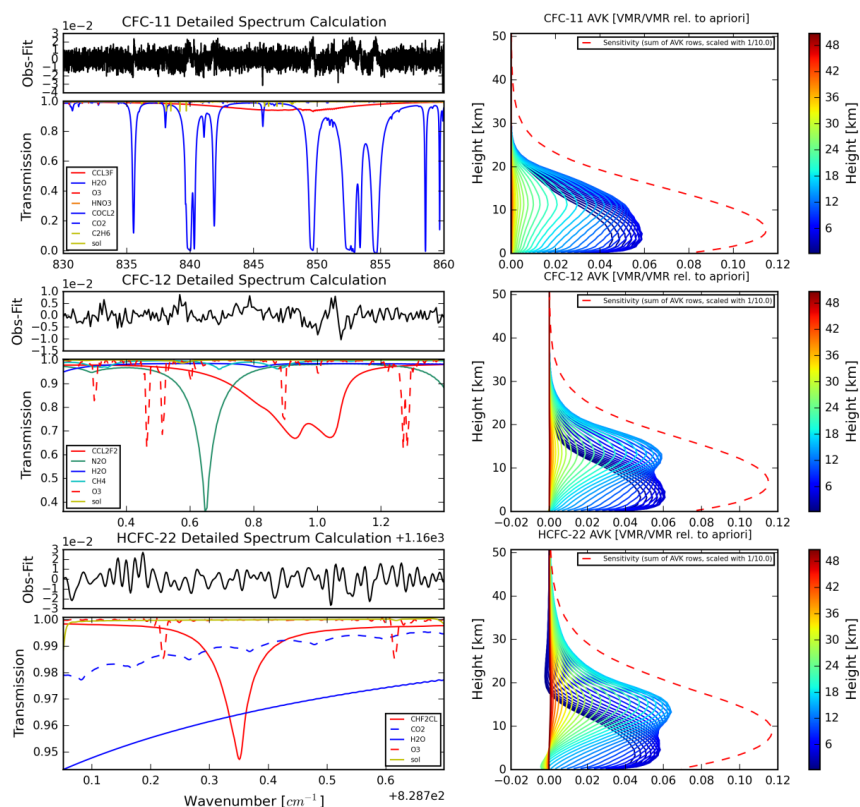
Figure 1. The typical spectrum and averaging kernels of CFC-11 (upper), CFC-12 (middle) and
HCFC-22 (bottom) at St Denis. The left panels show the transmission and residual (observed –
calculated spectrum) for the three retrieval microwindows, along with the absorption contribution
from each specie. Right panels show the averaging kernels for the target gases (no sensitivity
above 50 km). The solid lines represent the sensitivities at specific altitudes. The red dashed line is
the sum of the row of averaging kernel scaled with 0.1, indicating the vertical sensitivity.

Atmospheric
Measurement
Techniques
Open Access
EGU
Discussions
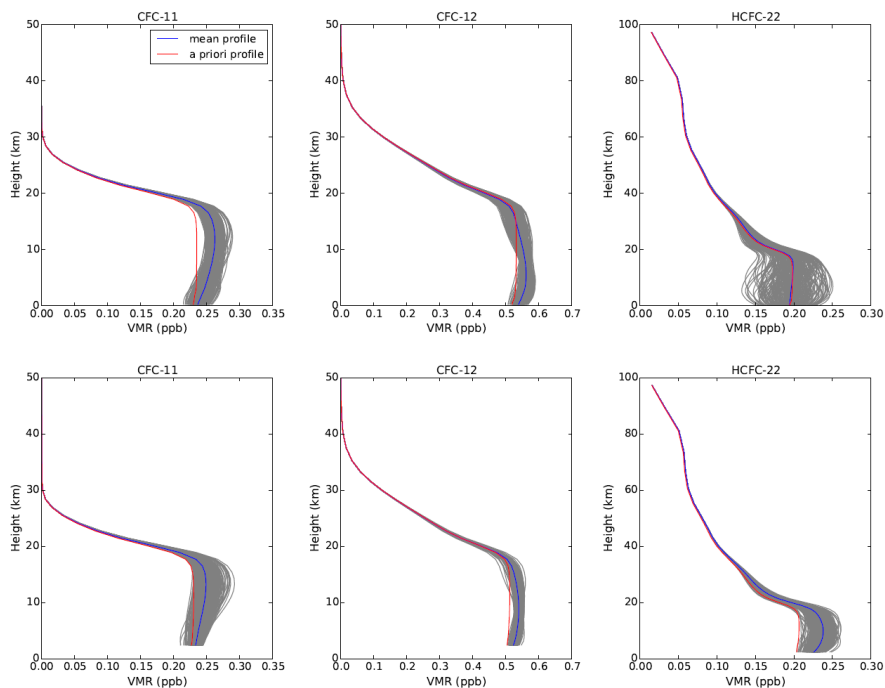
619

620   Figure 2. The a priori (red line), retrieved profiles (grey lines) and the mean retrieved profile (blue
621   line) of CFC-11, CFC-12 and HCFC-22 at St Denis (upper panels) and Maïdo (bottom panels).

Atmospheric
Measurement
Techniques

Open Access

Discussions

EGU

622
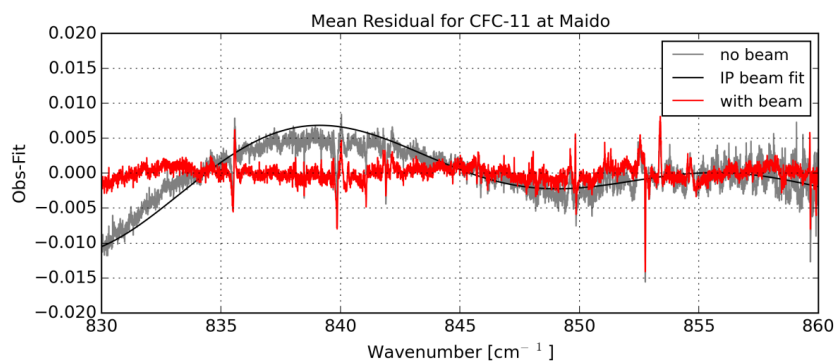
Figure 3. The mean residual transmittance (observed – calculated) of the CFC-11 retrievals with
and without beam parameters at Maïdo. The IP beam fit line is used as a priori IP beam
parameters.

Atmospheric
Measurement
Techniques
Discussions

Open Access

626
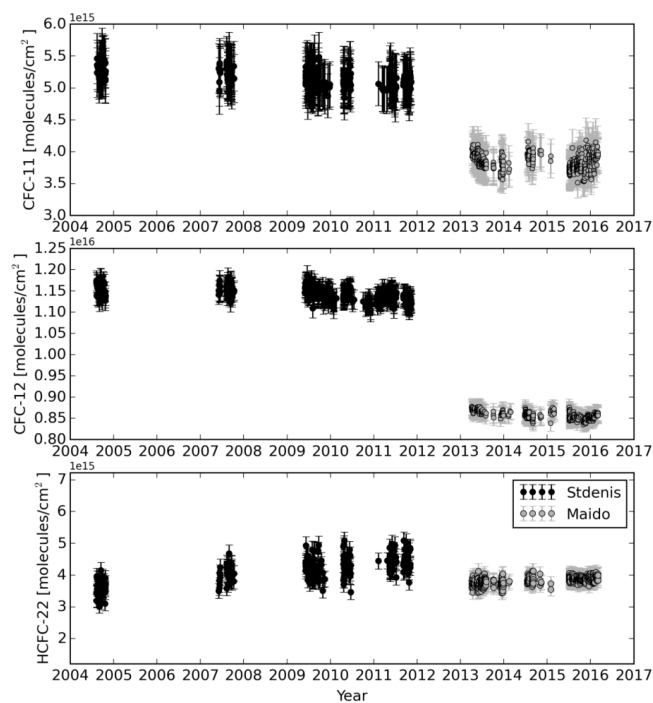
Figure 4. The time series of the total columns and total uncertainties of CFC-11, CFC-12 and
HCFC-22 at St Denis (black) and Maïdo (grey). The error bar contains both systematic and
random uncertainties from SFIT4 retrieval ($\sqrt{\varepsilon_s^2 + \varepsilon_r^2}$).

630
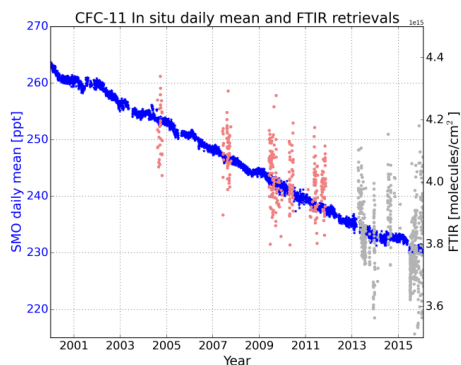
631
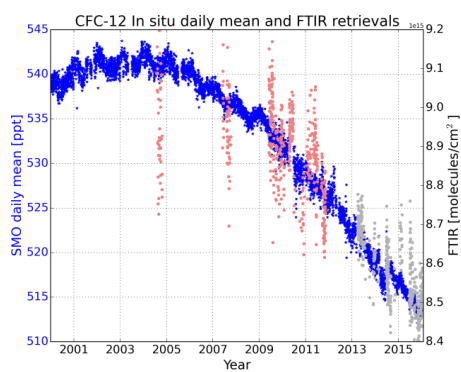
632
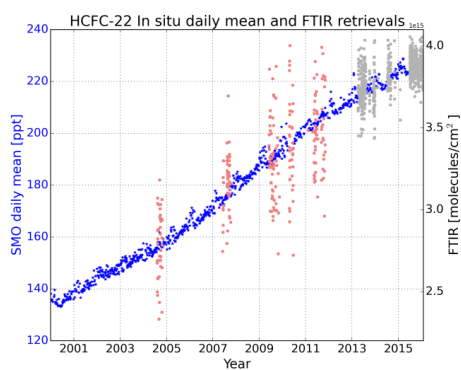
633 Figure 5. In-situ daily mean (CFC-11 and CFC-12) and flask pair measurements (HCFC-22) at
634 SMO site (blue) and individual FTIR partial column at St Denis (2.155-100 km; light coral) and
635 total column at Maïdo (2.155-100 km; grey). Upper: CFC-11; middle: CFC-12; bottom: HCFC-22.

636
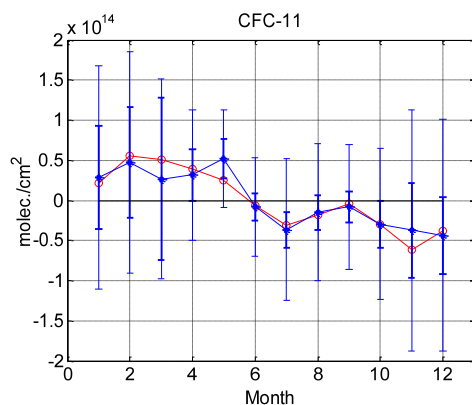
637
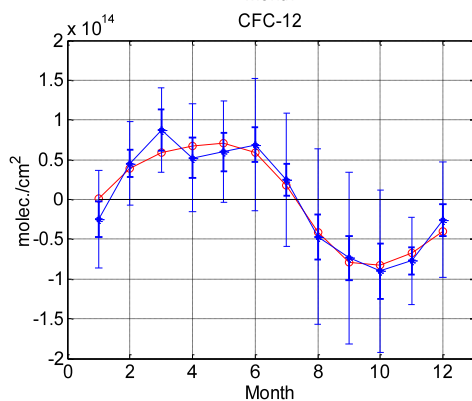
638
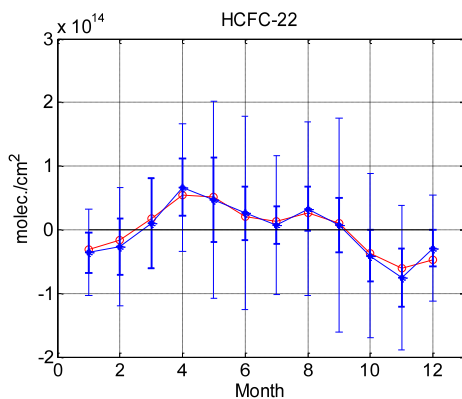
639   Figure 6: Seasonal cycles of CFC-11, CFC-12 and HCFC-22. The modelled seasonal cycle
640   obtained by Eq. 10 for the 2004-2016 St Denis -Maïdo time-series is shown in red. In blue, the
641   mean of FTIR measurements for each month during the 2004-2016 period, after subtraction of the
642   trend, is shown, together with the standard deviation σ of the mean (thin error bars). The 2 σ error
643   on the mean ($2\sigma / \sqrt{n}$; n being the number of measurements for each month) is also shown with
644   thick blue lines.

645
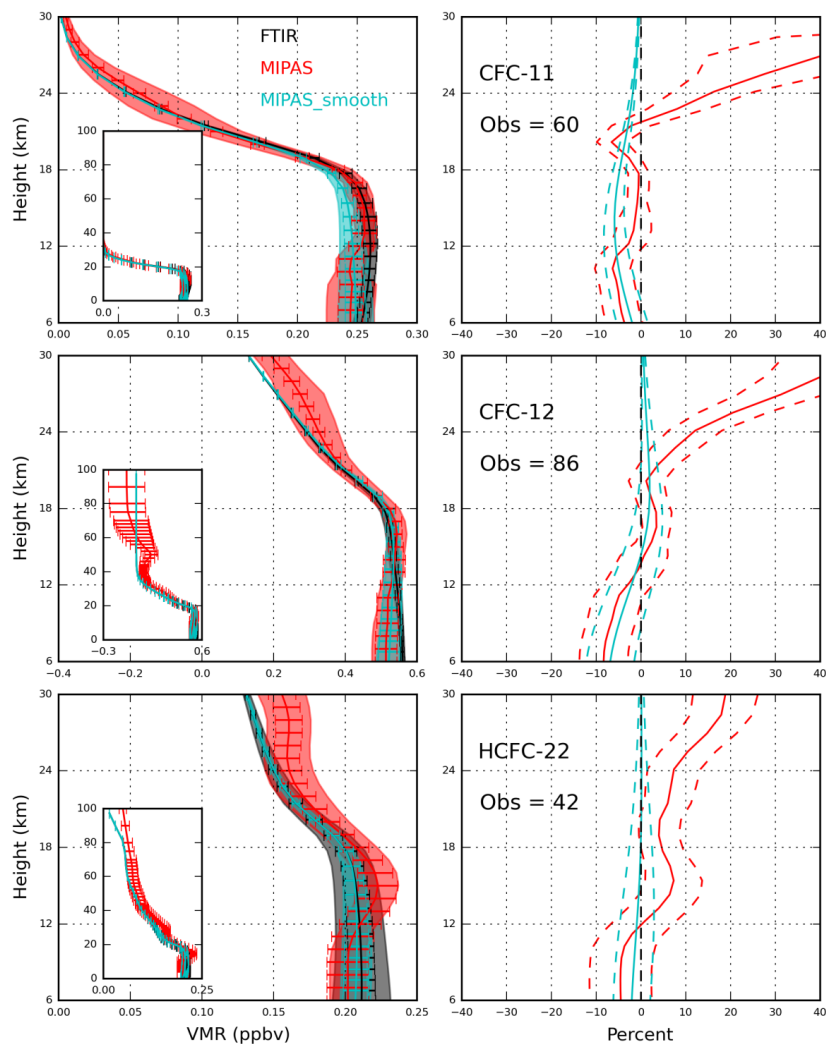
Figure 7. Left panel, for each target species (from top to bottom: CFC-11, CFC-12 and HCFC-22):
averaged target species mixing ratio profile, random uncertainty (error bar) and the standard
deviation of all the co-existing data pairs (shade area) for FTIR (in black) and for MIPAS (in red :
raw data; in sky blue: after smoothing with the corresponding FTIR averaging kernel). The
profiles (from 0 to 100 km) are also manifested in the left panels. Right panel, for each target
species, averaged relative difference between MIPAS and FTIR ((MIPAS − FTIR)/FTIR ×100%)
(solid lines), along with the standard deviation (dash lines).

Atmospheric
Measurement
Techniques
Discussions
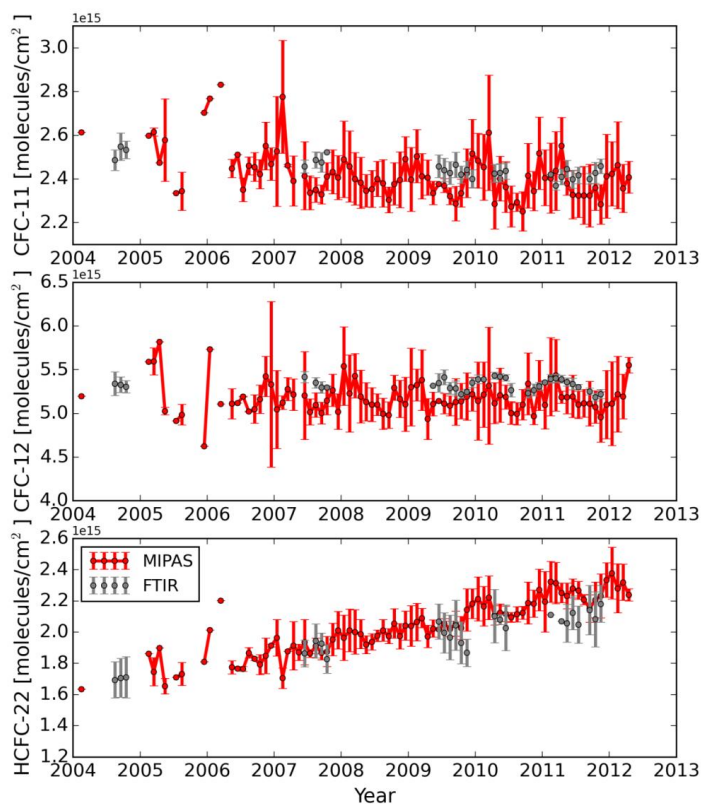
653

654   Figure 8. The time series of the monthly means of partial columns (6 to 30 km) of CFC-11,

655   CFC-12 and HCFC-22 from St Denis FTIR measurements (grey) and raw MIPAS data (red). Error

656   bars represent the standard deviations of the monthly means.